Central amygdala nucleus (Ce) gene expression linked to increased trait-like Ce metabolism and anxious temperament in young primates

Andrew S. Fox[a,b,c,1], Jonathan A. Oler[b,d], Steven E. Shelton[b,d], Steven A. Nanda[d], Richard J. Davidson[a,b,c,d], Patrick H. Roseboom[d], and Ned H. Kalin[a,b,c,d,1]

Departments of [a]Psychology and [d]Psychiatry and [b]HealthEmotions Research Institute, University of Wisconsin, Madison, WI 53719; and [c]Waisman Laboratory for Brain Imaging and Behavior, University of Wisconsin, Madison, WI 53705

Edited by Marcus E. Raichle, Washington University in St. Louis, St. Louis, MO, and approved September 11, 2012 (received for review April 23, 2012)

Children with anxious temperament (AT) are particularly sensitive to new social experiences and have increased risk for developing anxiety and depression. The young rhesus monkey is optimal for studying the origin of human AT because it shares with humans the genetic, neural, and phenotypic underpinnings of complex social and emotional functioning. In vivo imaging in young monkeys demonstrated that central nucleus of the amygdala (Ce) metabolism is relatively stable across development and predicts AT. Transcriptome-wide gene expression, which reflects combined genetic and environmental influences, was assessed within the Ce. Results support a maladaptive neurodevelopmental hypothesis linking decreased amygdala neuroplasticity to early-life dispositional anxiety. For example, high AT individuals had decreased mRNA expression of neurotrophic tyrosine kinase, receptor, type 3 (*NTRK3*). Moreover, variation in Ce *NTRK3* expression was inversely correlated with Ce metabolism and other AT-substrates. These data suggest that altered amygdala neuroplasticity may play a role the early dispositional risk to develop anxiety and depression.

positron-emission tomography | microarray | brain imaging

The ability to identify brain mechanisms underlying the risk during childhood for developing anxiety and depression is critical for establishing novel early-life interventions aimed at preventing the chronic and debilitating outcomes associated with these common illnesses. To this end, we have optimized a model of anxious temperament (AT), the conserved at-risk phenotype, in young developing rhesus monkeys (1–4). The rhesus monkey is ideal for studying the origin of human AT because these species share the genetic, neural, and phenotypic underpinnings of complex social and emotional functioning (5–10). Importantly, the rhesus developmental model bridges the critical gap between human psychopathology and rodent models, allowing for translation to humans by using in vivo imaging measures and translation to rodents by using ex vivo molecular methods. Thus, the unique hypotheses that can be generated from the rhesus model are invaluable in guiding both imaging studies in children and mechanistic efforts in rodents.

Of particular relevance to the AT rhesus model is the relatively recent evolutionary divergence between rhesus monkeys and humans (25 million years) compared with rodents and humans (70 million years) (5). This evolutionary closeness is reflected in the species' similarities in social and emotional behaviors. These homologies, instantiated in their conserved genetic and neural systems, underlie the ability of both humans and rhesus monkeys to form and maintain the relationships necessary for living in complex social environments. In this regard, the experience of anxiety has evolved in primates to motivate the formation of long-lasting attachment bonds that serve to increase security and group cohesion. The comparable rearing practices shared by these species (e.g., close mother–infant bonding) promote early social/emotional learning, which serves to adaptively regulate anxiety and promote survival (7).

Although periods of marked anxiety and fear are common during early childhood, most children overcome these anxieties through learning associated with experience and maturation. As they develop, typical children learn to discern real threats from distorted fears and, in concert, effectively regulate their behavior to adaptively cope. However, a subset of children with extreme AT do not develop this capacity, maintaining a stable anxious disposition that confers increased risk for the development of anxiety and mood disorders (11–13). AT begins as early shyness and is later characterized by chronic anxiety, negative affect, and worry (14). AT is also associated with increased activity of stress-sensitive peripheral systems, including increased pituitary–adrenal tone and heightened sympathetic activity (11).

Because early social-emotional learning is critical for the adaptive regulation of anxiety, we have been especially interested in processes demonstrated to underlie learning during development. Furthermore, recent preclinical and clinical research has identified neurotrophic factors (15) and other neuroplastic processes as critical for overcoming adult psychopathology (16–18). Therefore, we hypothesized that altered neurotrophic processes in the young brain would lead to the emergence and maintenance of childhood AT. In particular, we theorize that deficits in the ability to modify the connections and composition of AT's neural substrate could result in a failure to learn how to adaptively regulate anxiety, which can manifest as a tendency to generalize perceptions of threat to neutral stimuli. Because AT can be identified early in life, characterizing the biological factors that promote the maintenance of stable AT can potentially lead to targeted early-life interventions aimed at decreasing the risk for developing psychopathology.

Similar to anxious children, young monkeys with high levels of AT are those that show increased freezing, decreased vocalizations, and increased cortisol when exposed to the no-eye contact condition (NEC) of the human-intruder paradigm, an ethologically relevant mild social threat. Our studies demonstrated that, like human AT, monkey AT is trait-like and heritable (19). Using functional brain imaging in conjunction with ex vivo molecular analyses of relevant brain regions, the monkey model allows for the longitudinal study of AT and its underlying neural substrates. With functional brain imaging, we identified the central nucleus of the amygdala (Ce) and anterior hippocampus as components of the neural circuit underlying AT (2, 19). More-

Author contributions: S.E.S., R.J.D., P.H.R., and N.H.K. designed research; A.S.F., S.E.S., S.A.N., P.H.R., and N.H.K. performed research; A.S.F. contributed new reagents/analytic tools; A.S.F., J.A.O., P.H.R., and N.H.K. analyzed data; and A.S.F., J.A.O., and N.H.K. wrote the paper.

The authors declare no conflict of interest.

This article is a PNAS Direct Submission.

[1]To whom correspondence may be addressed. E-mail: asfox@wisc.edu or nkalin@wisc.edu.

This article contains supporting information online at www.pnas.org/lookup/suppl/doi:10.1073/pnas.1206723109/-/DCSupplemental.

over, we found that young primates with high AT have increased metabolism in these regions when studied in both stressful and nonstressful contexts (2). These data set the stage for in-depth molecular studies in primates focused on understanding the mechanisms mediating the function of the brain regions underlying AT.

The Ce is of interest because its efferent projections coordinate autonomic, hormonal, behavioral, and emotional responses to stress (20), and Ce lesions in monkeys are sufficient to reduce AT (21). Furthermore, rodent studies demonstrate that direct Ce manipulations markedly alter unconditioned anxiety responses (22), similar to those elicited by novel or potentially threatening situations in children with high AT. The prefrontal cortex and other amygdala nuclei primarily influence fear and anxiety-related responding via the Ce, where intra-Ce microcircuits play a critical role dynamically gating these inputs (23–26). Recent work in rhesus monkeys demonstrates that, unlike most amygdala nuclei, the Ce continues to mature from the first year of life into early adulthood (27). This protracted developmental period suggests that Ce maturation may be particularly susceptible to environmental influences. A causal relation between social group size and dorsal amygdala volume demonstrates the importance of social influences on the primate amygdala (28). These findings are consistent with our data highlighting the importance of environmental contributions to Ce metabolism as it relates to early-life AT (19). For these reasons, we selected the Ce for in depth molecular analyses, with a particular focus on processes within the Ce that underlie learning. Although learning-related research has generally focused on the hippocampus (e.g., refs. 29 and 30) and basal/lateral amygdala regions (31), recent rodent studies highlight the role of plasticity and emotional learning in the Ce (32, 33). In addition to its role in anxiety, the Ce has recently been linked to habit formation (34) and, at a cellular and neurochemical level, it has much in common with the striatum (35), a structure known to mediate the development of long-term ingrained response patterns (36). Although Ce microcircuits are ideally suited to perform the childhood learning that results in adaptive anxiety, when Ce learning is disrupted, it could result in trait-like habitual fear and anxiety responding.

Building on our finding that individual differences in Ce metabolism predict AT, we performed mRNA expression studies in Ce tissue collected from young monkeys repeatedly phenotyped for AT and its associated brain metabolism. This unique, multilevel approach combines the power of functional brain imaging with the potential of gene expression studies to characterize the mRNAs that could underlie the risk for developing anxiety and depression. We hypothesized that high-AT individuals would have alterations in mRNAs within the Ce that reflect the influences of experience on the persistent expression of anxiety. Specifically, we predicted a role for mRNAs encoding molecules with the potential to facilitate habitual anxiety and developmentally appropriate adaptive fear learning. Such alterations are of particular interest, because manipulations of these substrates could result in treatments for high-AT children that would facilitate their ability to modify and adaptively regulate their anxiety.

Accordingly, a subset of 24 animals was selected from 238 rhesus monkeys that were initially characterized for behavior and brain metabolism. The 238 monkeys were injected with [^{18}F]-fluoro-2-deoxyglucose (FDG) and exposed for 30 min to the NEC condition that elicits the AT phenotype (19). During NEC, a human ("the intruder") enters the test room and presents her profile to the monkey, avoiding eye contact (1). Following NEC exposure, animals were anesthetized, and high-resolution positron-emission tomography (PET) scans were performed to examine the integrated brain metabolism that occurred during the preceding 30-min NEC exposure. FDG-PET is optimal for simultaneously assessing sustained neural activity and natural behavior in unconstrained individuals because FDG is taken up into metabolically active cells over the course of ∼30 min and remains trapped for the duration of its ∼110-min half-life. This extended assessment of brain metabolism is ideal for studying the neural underpinnings of AT, which are sustained over time.

Results and Discussion

The subset of 24 males underwent further testing to characterize the trait-like components of AT and its neural substrate across development [Fig. 1*A*; animals noted in pink constituted the subset that was further tested; age at first assessment: mean, 2.1 (range, 0.85–3.5 y); age at last assessment: mean, 3.2 (range, 1.8–4.2)]. The age span of this sample is similar to childhood through early adolescence in humans because 1-y-old monkeys are similar to 3- to 4-y-old children, and male monkeys enter adolescence around 3–4 y of age. The 24 monkeys were phenotyped for brain and behavior on two additional occasions, 6–18 mo after their initial assessment. Between the second and third assessment, half of the animals were relocated every 5 d over a period of 3 wk. Relocation did not have any significant effects on behavior or physiology (*SI Methods*). To examine the stability of AT, we tested the interrelations among the three repeated measurements, controlling for relocation, age, and interval between assessments. Relations among the AT measures were significant [time 1 to time 2: $t = 6.83$, $P < 0.0001$; time 1 to time 3: $t = 3.80$, $P = 0.001$; time 2 to time 3: $t = 5.16$, $P < 0.0001$; accounting for between 44% and 72% of the variance in AT across time points and corresponding to an interclass correlation coefficient $(ICC)_{3,1} = 0.72$], confirming AT's relative stability over this developmental period.

We hypothesized that the stability of AT would be reflected by similar consistency in the function of its neural substrates. Therefore, we intercorrelated the three measures of NEC-induced brain metabolism in the regions predictive of AT, controlling for relocation, age, and interval between assessments. AT-predictive regions were defined from our previous study and included bilateral anterior temporal lobe clusters, bilateral occipital lobe clusters, and a midline parietal lobe cluster (19). Results demonstrated relative stability as denoted by significant interrelations among the three NEC-induced metabolism measurements within each of these clusters [corrected for multiple comparisons using false discovery rate (FDR); $q < 0.05$ FDR across maps in AT-related regions, with voxel-wise $ICC_{3,1}$ coefficients ranging from 0.30 to 0.70 (median, 0.57); Fig. 1*B* and Table S1]. Voxels within every cluster we tested, including dorsal and ventral regions of amygdala, anterior portions of hippocampus, superior temporal sulcus (STS), agranular insula, temporal and insular proisocortices, claustrum, visual cortex, and precuneus, demonstrated significantly stable NEC-induced metabolism. These data demonstrate that individual differences in metabolism within the neural circuit underlying AT are relatively stable across juvenile development.

We next examined covariation between the stable components of AT and its neural substrates. For each animal, the stable components of AT and regional brain metabolism were estimated by computing their means across each of the three longitudinal assessments. Mean AT was regressed against mean voxel-wise metabolism in significantly stable AT-related regions, while controlling for relocation, age, the interval between scans, and voxel-wise gray matter probability (GMP). Results demonstrated that mean metabolism in amygdalar regions (including Ce and the basolateral complex), anterior hippocampus, and visual cortex predicted mean AT ($q < 0.05$ FDR in stable AT-related regions; Fig. 1 *C* and *D* and Table S2). To confirm involvement of the Ce within the larger amygdalar cluster we assessed the overlap between this cluster and a map of in vivo serotonin transporter binding derived from separate animals (37). Precise localization of the Ce can be determined with this method because this amygdalar nucleus has the highest density of serotonin transporter binding compared with neighboring structures (38) (*SI Methods*). Results confirmed that mean

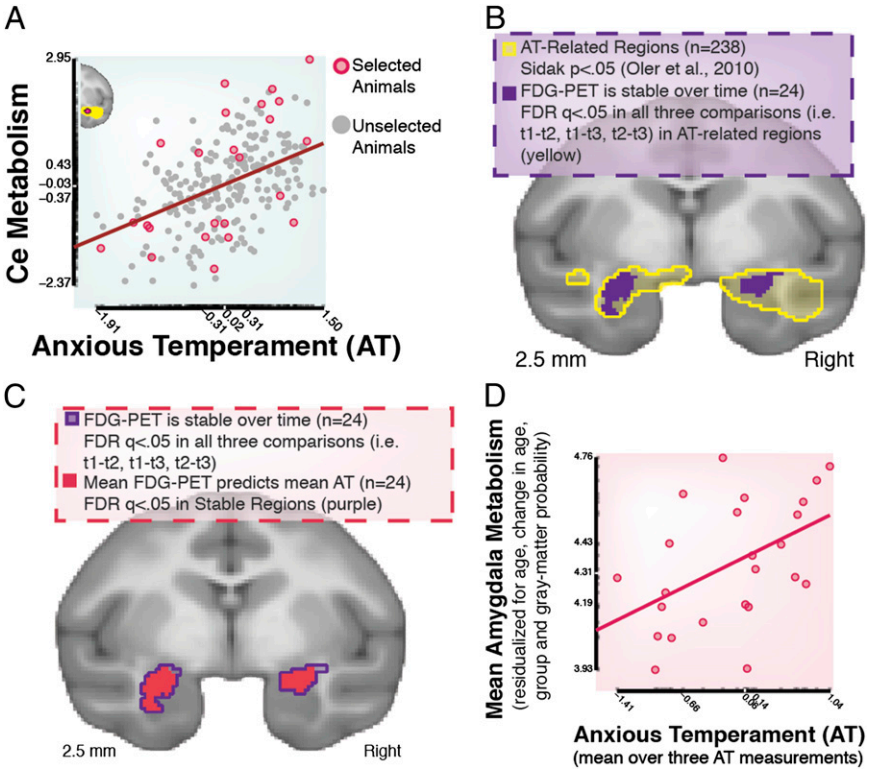

Fig. 1. Stable amygdala metabolism predicts dispositional AT. (*A*) In a large cohort of monkeys (n = 238), we identified regions in which metabolic activity predicted AT [yellow; see Oler et al. (19)]. In yellow is the anterior temporal lobe cluster, which encompasses the Ce region (red) most predictive of AT. As can be seen in the regression plot, 24 animals (pink dots) were selected to represent the full range of variability in AT and Ce metabolism. (*B*) Longitudinal assessments of brain metabolism in the 24 animals demonstrate that portions of the temporal lobe clusters are stable over time (purple) [FDR-corrected within AT-related regions defined by Oler et al. (19) (yellow) for three pairwise stability tests, i.e., T1-T2, T2-T3, T1-T3]. (*C*) Mean longitudinal assessments of brain metabolism and AT were significantly correlated (pink) within the region where metabolism was stable (FDR-corrected within the purple region of stability from *B*). (*D*) Scatterplot depicting relations between metabolism within the amygdala region (pink) depicted in *C* and mean AT residualized for relocation, age and interval between assessments (r = 0.47; P = 0.0377).

metabolism in the Ce region predicted mean AT across assessments. This longitudinal assessment of brain and behavior extends prior work characterizing the neural substrates of AT by demonstrating that the trait-like nature of AT is reflected in trait-like metabolism within the Ce and other AT-related brain regions.

To characterize the molecular underpinnings of AT and its neural substrate, animals were killed and brain tissue was collected for assessment of gene expression. Because of our interest in the trait-like nature of AT and its context-independent brain metabolism, we collected brain tissue from animals in their baseline state, 4–5 d following final NEC exposure. In contrast to studies of stimulus-evoked gene expression, this approach allows for optimal characterization of temperament-related transcripts. mRNA was extracted from the Ce region most predictive of AT (n = 238; Figs. 1*A* and 2). mRNA expression levels were assessed using the Affymetrix Rhesus Monkey microarray (*SI Methods*). Brain samples collected were counterbalanced for hemisphere because bilateral Ce metabolism was associated with AT. To quantify the association between dispositional AT and Ce mRNA levels, mean AT was correlated with mRNA expression levels. Microarray data were analyzed using bioconductor (39) for microarray analysis in R (see *SI Methods* for details). Microarray data were preprocessed using robust multichip average (RMA) background correction, constant normalized across chips, and summarized across probes using the median-polish technique (40). Resulting gene expression levels were visually inspected using MA plots (Fig. S1). Gene expression was also assessed using Plier background correction and quantile normalization to verify that gene distribution patterns did not arise from specific preprocessing techniques (i.e., Plier and quantile normalization). Robust regression analyses between mean AT- and RMA-determined mRNA levels (controlling for relocation, biopsy hemisphere, and age) were performed on annotated transcripts (http://www.unmc.edu/rhesusgenechip/) that had at least moderate expression levels [>log2(100)]. Covarying for age ensures that significant AT-related transcripts, although assessed during development, are not reflective of age-related changes. The empirical Bayes method was used to determine levels of significance and the FDR was used to account for multiple comparisons.

Results revealed 139 RMA-determined transcripts that predicted AT (FDR $q < 0.05$, two-tailed; Table S3; to demonstrate these correlations are not attributable to the normalization technique, Table S3 also includes the correlations between AT and Plier background corrected and quantile normalized transcripts). Consistent with the concept that multiple systems underlie stress-related psychopathology, both manual inspection and gene-ontology enrichment analyses revealed that the 139 FDR-corrected AT-related transcripts reflect diverse biological systems (*SI Methods* and Table S4). Within the Biological Processes ontology, 35 significantly overrepresented terms were identified. Three of these terms are of particular interest in relation to our maladaptive neurodevelopmental hypothesis of AT. These include response to hormone stimulus (GO:0009725) and related terms, positive regulation of axon extension (GO:0045773), and positive regulation of developmental growth (GO:0048639). Of note, the neurotrophic tyrosine kinase, receptor, type 3 (NTRK3) and the leucine-rich repeat protein ISLR2 (Ig superfamily containing leucine-rich repeat 2; also known as Linx) are the only constituents from the FDR corrected list of 139 genes that are represented across all 3 terms. Because multiple comparison correction of AT-related transcripts likely results in false negatives and the possibility that the exclusion of these genes can alter ontology term representation, we also performed gene-ontology enrichment analyses on significantly ($P < 0.05$) uncorrected AT-related genes. Although not identical, the results support the inferences of the FDR-corrected ontology analyses (Table S5). Significantly overrepresented terms included regulation of axon regeneration (GO:0048679) and cell morphogenesis (GO:0000902), both of which included NTRK3. Although future research would benefit from exploring other significantly AT-related genes and overrepresented ontology terms, because of our theoretical interest in the mechanisms of Ce-learning during

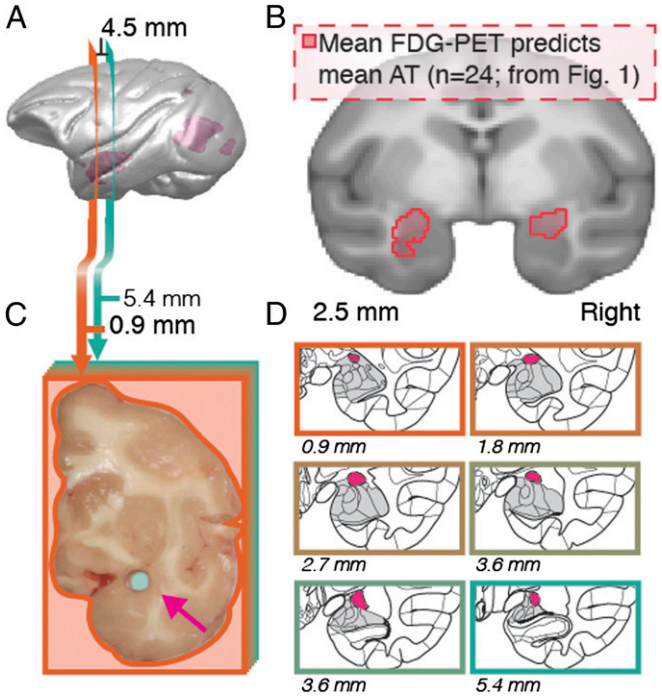

Fig. 2. Stable Ce regions predictive of dispositional AT were used to guide amygdala biopsy. (*A*–*C*) Brains from the 24 animals were sectioned into 4.5-mm coronal slabs centered on the functionally defined amygdala region (~0.9 mm [orange] to ~5.4 mm [cyan], posterior to anterior commissure), shown as a 3D rendering (*A*), a 2D slice through the functionally defined amygdala region (*B*), and a representative single-subject slab with amygdala biopsy site (magenta arrow) (*C*). (*D*) The biopsied region corresponds to the location of Ce (pink), as shown in the series of atlas slices [adapted with permission (69)]. Slices are arranged from anterior (orange) to posterior (cyan).

development, we focused our analyses on NTKR3 and related transcripts. Quantitative real-time PCR (qRT-PCR) was performed on select transcripts including NTRK3, IRS2, and ISLR2 (*P* values, <0.05) to confirm the relations between gene expression and AT.

NTRK3 and insulin receptor substrate 2 (*IRS2*) are of particular interest because their activation by the endogenous growth factor neurotrophin-3 (*NTF-3*) can initiate synaptogenesis and neurogenesis (41, 42) (Fig. 3). The *NTRK3* gene encodes a membrane-bound receptor that phosphorylates intracellular transducers, including *IRS2* (43). The downstream influences of *IRS2* can manifest via activation of the phosphoinositide 3-kinase/protein kinase B (*PI3K/AKT*) pathway (44). *AKT* signaling affects synaptic plasticity, axonal development, amygdala-dependent learning, and behavioral responses to stress (45, 46). Additionally, ISLR2 sits on the cell membrane, aids in the guiding of axons, and can facilitate the activation of trk receptors, including NTRK3 (47, 48). In addition to its involvement in our theoretically motivated focus on neuroplasticity, *NTRK3* genetic variation has been linked to human psychopathology, including childhood-onset mood disorders (49–52), and via its extracellular domain may provide an accessible drug target. Taken together, these findings implicate NTRK3 as a prominent target for future mechanistic studies examining childhood AT.

Using the prospectively acquired trait-like measures of brain metabolism, we investigated the neural systems by which altered Ce NTRK3 expression influences AT. A voxel-wise search, controlling for age, hemisphere of biopsy, relocation, and GMP, was performed to identify AT-related brain regions in which Ce *NTRK3* mRNA levels predicted mean metabolic activity. Results demonstrated significant negative relationships between Ce *NTRK3* expression and glucose metabolism within the right amygdala (including the Ce region) and anterior hippocampus, as well as significant positive relations within visual cortex (Fig. 4; FDR $q <$ 0.05 in stable AT-predictive regions; Table S6). Although the left Ce region did not survive multiple comparison correction, the relationship between NTRK3 expression and left Ce metabolism was significant at an uncorrected $P = 0.02$, which was not significantly weaker than the relationship between NTRK3 expression and right Ce metabolism ($t = 0.86$; $P = 0.40$) (53). These primate data combine the use of brain imaging and microarray technology in the same animals and suggest that Ce *NTRK3* is a key molecular mediator of AT via its influences on the neural circuit underlying AT.

To examine the unique relation between Ce NTRK3 expression and AT, we assessed motor cortex NTRK3 mRNA. Results demonstrated that motor cortex *NTRK3* mRNA levels were unrelated to Ce *NTRK3* mRNA levels ($t = 0.09$; $P = 0.928$). Moreover, motor cortex *NTRK3* mRNA levels were not related to AT ($t = 0.24$; $P = 0.812$) nor metabolism in AT-related regions (no

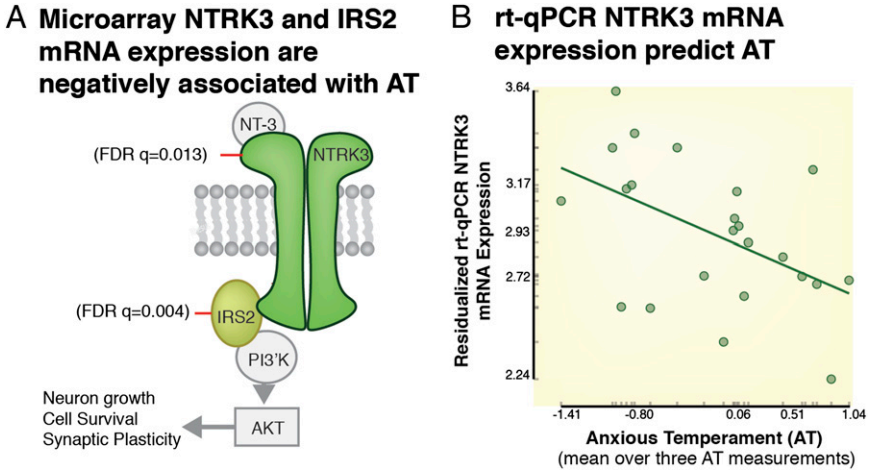

Fig. 3. Ce expression of the neurotrophic receptor NTRK3 predicts AT. (*A*) Schematic of the pathway for *NTRK3*, a neuroplasticity-associated molecule (green). Microarray data showed that individuals with higher levels of Ce *NTRK3* mRNA expression exhibited lower AT. A similar pattern was found for a downstream target of *NTRK3*, *IRS2* (yellow). Other molecules in the *NTRK3* pathway are depicted in gray. (*B*) qRT-PCR confirmed the negative relationship between Ce *NTRK3* mRNA expression levels and AT, controlling for relocation, biopsy hemisphere, and age ($r = 0.49$; $P = 0.029$).

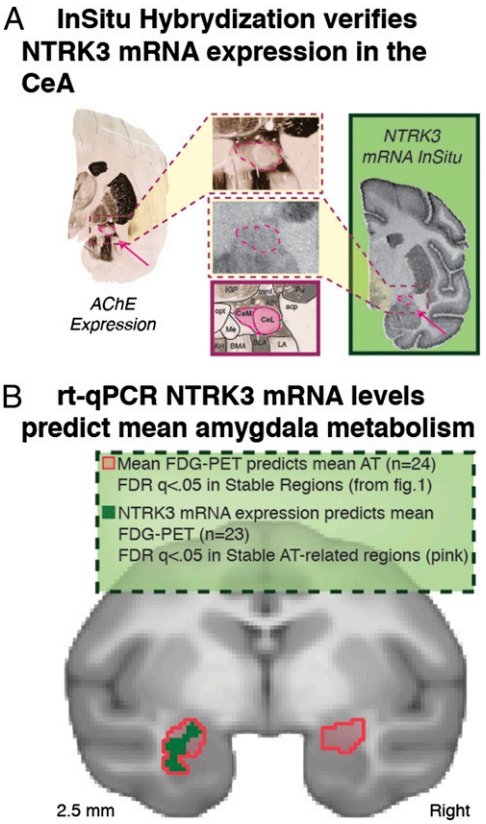

Fig. 4. NTRK3 is expressed in Ce and negatively predicts Ce metabolism. (*A*) Acetylcholinesterase (AChE) stain (*Left*) was used to definitively identify Ce in the brain of one subject. In situ hybridization of *NTRK3* was performed on an adjacent slice from the same subject (*Right*). Magnified insets (*Center*) reveal that the AChE-defined Ce (dashed-pink) expresses *NTRK3* mRNA. (*B*) Individuals showing higher levels of *NTRK3* mRNA expression, indexed by qRT-PCR, show reduced Ce metabolism in vivo (green) [FDR-corrected within the stable AT-related region (pink)].

significant results at FDR $q < 0.05$). Although motor cortex metabolism was highly predictive of levels of locomotion ($P < 0.05$, Sidak-corrected; *SI Methods* and Table S7), motor cortex *NTRK3* mRNA expression was not significantly correlated with either locomotion ($t = -1.31$; $P = 0.190$) or motor cortex metabolism (no significant results at FDR $q < 0.05$; *SI Methods*). These findings demonstrate that regional *NTRK3* mRNA expression is not a general marker for brain metabolism nor is it a nonspecific reflection of behaviors dependent on the region in which *NTRK3* mRNA is assessed (e.g., locomotion for motor cortex). This further underscores the specificity of Ce *NTRK3* in relation to AT and highlights the importance of site-specific, differential regulation of the *NTRK3* gene.

Our results highlight the role of *NTRK3* in AT during development but do not implicate NTRK3 mechanistically. Rather, these findings provide an initial rationale for exploring behavioral or pharmacological interventions aimed at up-regulating regional *NTRK3* expression early in the lives of individuals likely to develop anxiety and depressive disorders. Recent studies in rodents demonstrate the feasibility of performing early targeted interventions that have long-term impacts on anxiety and adaptive responses to stress (54–56). For example, neonatal injections of the neuroplasticity-related growth factor fibroblast growth factor 2 (*FGF2*) altered the developmental trajectory of high-anxious rodents, resulting in decreased adult anxiety (55). Importantly, early-life *FGF2* treatment also enhanced adult neurogenesis, which was accompanied by increased hippocampal expression of *NTRK3* (55). Moreover, primate research has demonstrated that neurodevelopmentally relevant gene expression in the amygdala is altered by prolonged maternal separation (57). Taken together, these data are consistent with our demonstration that monkeys with lower levels of AT show greater Ce expression of *NTRK3* and further motivate mechanistic research into the role for neurodevelopmentally important transcripts in the development of AT.

Although we focus on NTRK3, it is important to clarify that other genes are also of interest. For example, in addition to its importance in neurotrophic signaling, the involvement of IRS2, which is also critical for insulin signaling, is interesting in its own right. Because of its multiple functions, regulation of IRS2 may be important in the linkages between stress, psychopathology, and the development of associated physiological alterations such as metabolic syndrome and type 2 diabetes. In the periphery, IRS2 regulates insulin sensitivity and in the brain IRS2 impacts multiple functions including reward (58), memory (59, 60), and energy homeostasis (61, 62). Moreover, type 2 diabetes has been associated with amygdala atrophy (63), and bidirectional associations between insulin resistance and affective disorders have been reported (64–66). The possibility that altered IRS2 function may play a role in the associations between insulin-related disorders and alterations in stress-related psychopathology via its effects on the amygdala is intriguing. Of particular interest to stress and AT, alterations in cortisol could be important in modulating IRS2 function because the synthetic glucocorticoid dexamethasone prevents phosphorylation of IRS2 (67, 68).

Recent work demonstrating the ongoing development of the primate Ce suggests this nucleus to be particularly susceptible to environmental influences throughout childhood and adolescence (19, 27). Early in childhood, as young children first extend beyond their parents' reach, they must approach novelty with trepidation. By way of experience and maturation, most children learn to regulate their anxieties and see the world as an opportunity for exploration. This experience-dependent learning results in refined discrimination between threatening and nonthreatening stimuli and likely involves sculpting of intra-Ce connections that dynamically gate the sensory and prefrontal triggers of fear. We hypothesize that decreased capacity for learning and modification within the Ce microcircuit could explain why some children fail to regulate their anxieties and develop an extreme anxious temperament. The findings presented here begin to link specific experience-dependent molecular pathways within the Ce to chronically elevated Ce metabolism and extreme temperamental anxiety. Although there are likely many mediators of AT, these gene expression data are consistent with a maladaptive neurodevelopmental hypothesis as a basis for AT. Future work should aim to extend these data in support of a molecular-neuroscientific rationale for conceptualizing new treatment strategies aimed at normalizing Ce function in vulnerable children before the development of the detrimental behavioral, emotional, and brain sequelae associated with the long-term consequences of chronic anxiety and depression.

Methods

Twenty-four male rhesus monkeys were selected from subjects used by Oler et al. (19) to undergo longitudinal AT and FDG-PET assessments during exposure to potential threat (NEC). Brain tissue was biopsied from the Ce region most predictive of AT, and transcriptome wide RNA expression levels were assessed using Affymetrix GeneChip Rhesus Macaque Genome arrays. All preprocessing and statistical analyses were performed using standard methods. See *SI Methods* for a detailed description of the procedures used.

ACKNOWLEDGMENTS. We thank the staff at the Wisconsin National Primate Center, the Harlow Center for Biological Psychology, the HealthEmotions Research Institute, and The Waisman Laboratory for Brain Imaging and Behavior for facilitating our research. We also thank A. Shackman, A. Alexander, B. Christian, L. Ahlers, A. Converse, T. Oakes, H. Van Valkenberg, K. Myer,

J. Spears, E. Larson, and D. French for their technical and analytic assistance in running subjects and analyzing data. This work was supported by National Institutes of Health (NIH) Grants MH91550, MH046729, MH081884, MH084051, HD008352, and HD003352; NIH Training Grant MH018931; the Wisconsin National Primate Research Center (through NIH Grants P51OD011106 and P51RR000167); and the HealthEmotions Research Institute.

1. Kalin NH, Shelton SE (1989) Defensive behaviors in infant rhesus monkeys: Environmental cues and neurochemical regulation. *Science* 243:1718–1721.
2. Fox AS, Shelton SE, Oakes TR, Davidson RJ, Kalin NH (2008) Trait-like brain activity during adolescence predicts anxious temperament in primates. *PLoS ONE* 3:e2570.
3. Fox AS, et al. (2005) Calling for help is independently modulated by brain systems underlying goal-directed behavior and threat perception. *Proc Natl Acad Sci USA* 102: 4176–4179.
4. Kalin NH, Shelton SE, Fox AS, Oakes TR, Davidson RJ (2005) Brain regions associated with the expression and contextual regulation of anxiety in primates. *Biol Psychiatry* 58:796–804.
5. Gibbs RA, et al.; Rhesus Macaque Genome Sequencing and Analysis Consortium (2007) Evolutionary and biomedical insights from the rhesus macaque genome. *Science* 316:222–234.
6. Kalin NH, Shelton SE (2003) Nonhuman primate models to study anxiety, emotion regulation, and psychopathology. *Ann N Y Acad Sci* 1008:189–200.
7. Harlow HF (1958) The nature of love. *Am Psychol* 13:673–685.
8. Adolphs R (2010) What does the amygdala contribute to social cognition? *Ann N Y Acad Sci* 1191:42–61.
9. Wallis JD (2012) Cross-species studies of orbitofrontal cortex and value-based decision-making. *Nat Neurosci* 15:13–19.
10. Chareyron LJ, Banta Lavenex P, Amaral DG, Lavenex P (2011) Stereological analysis of the rat and monkey amygdala. *J Comp Neurol* 519:3218–3239.
11. Fox NA, Henderson HA, Marshall PJ, Nichols KE, Ghera MM (2005) Behavioral inhibition: Linking biology and behavior within a developmental framework. *Annu Rev Psychol* 56:235–262.
12. Biederman J, et al. (2001) Further evidence of association between behavioral inhibition and social anxiety in children. *Am J Psychiatry* 158:1673–1679.
13. Essex MJ, Klein MH, Slattery MJ, Goldsmith HH, Kalin NH (2010) Early risk factors and developmental pathways to chronic high inhibition and social anxiety disorder in adolescence. *Am J Psychiatry* 167:40–46.
14. Kagan J, Reznick JS, Snidman N (1988) Biological bases of childhood shyness. *Science* 240:167–171.
15. Martinowich K, Manji H, Lu B (2007) New insights into BDNF function in depression and anxiety. *Nat Neurosci* 10:1089–1093.
16. Krystal JH, et al. (2009) Neuroplasticity as a target for the pharmacotherapy of anxiety disorders, mood disorders, and schizophrenia. *Drug Discov Today* 14:690–697.
17. Manji HK, Moore GJ, Rajkowska G, Chen G (2000) Neuroplasticity and cellular resilience in mood disorders. *Mol Psychiatry* 5:578–593.
18. Pittenger C, Duman RS (2008) Stress, depression, and neuroplasticity: A convergence of mechanisms. *Neuropsychopharmacology* 33:88–109.
19. Oler JA, et al. (2010) Amygdalar and hippocampal substrates of anxious temperament differ in their heritability. *Nature* 466:864–868.
20. Davis M, Whalen PJ (2001) The amygdala: Vigilance and emotion. *Mol Psychiatry* 6: 13–34.
21. Kalin NH, Shelton SE, Davidson RJ (2004) The role of the central nucleus of the amygdala in mediating fear and anxiety in the primate. *J Neurosci* 24:5506–5515.
22. Tye KM, et al. (2011) Amygdala circuitry mediating reversible and bidirectional control of anxiety. *Nature* 471:358–362.
23. Ehrlich I, et al. (2009) Amygdala inhibitory circuits and the control of fear memory. *Neuron* 62:757–771.
24. Ciocchi S, et al. (2010) Encoding of conditioned fear in central amygdala inhibitory circuits. *Nature* 468:277–282.
25. Haubensak W, et al. (2010) Genetic dissection of an amygdala microcircuit that gates conditioned fear. *Nature* 468:270–276.
26. Pare D, Duvarci S (2012) Amygdala microcircuits mediating fear expression and extinction. *Curr Opin Neurobiol* 22:717–723.
27. Chareyron LJ, Lavenex PB, Amaral DG, Lavenex P (2012) Postnatal development of the amygdala: A stereological study in macaque monkeys. *J Comp Neurol* 520:1965–1984.
28. Sallet J, et al. (2011) Social network size affects neural circuits in macaques. *Science* 334:697–700.
29. Kim JJ, Diamond DM (2002) The stressed hippocampus, synaptic plasticity and lost memories. *Nat Rev Neurosci* 3:453–462.
30. Ming G-L, Song H (2011) Adult neurogenesis in the mammalian brain: Significant answers and significant questions. *Neuron* 70:687–702.
31. Fanselow MS, LeDoux JE (1999) Why we think plasticity underlying Pavlovian fear conditioning occurs in the basolateral amygdala. *Neuron* 23:229–232.
32. Paré D, Quirk GJ, Ledoux JE (2004) New vistas on amygdala networks in conditioned fear. *J Neurophysiol* 92:1–9.
33. Samson RD, Duvarci S, Paré D (2005) Synaptic plasticity in the central nucleus of the amygdala. *Rev Neurosci* 16:287–302.
34. Lingawi NW, Balleine BW (2012) Amygdala central nucleus interacts with dorsolateral striatum to regulate the acquisition of habits. *J Neurosci* 32:1073–1081.
35. Swanson LW, Petrovich GD (1998) What is the amygdala? *Trends Neurosci* 21: 323–331.
36. Packard MG, Knowlton BJ (2002) Learning and memory functions of the Basal Ganglia. *Annu Rev Neurosci* 25:563–593.
37. Christian BT, et al. (2009) Serotonin transporter binding and genotype in the nonhuman primate brain using [C-11]DASB PET. *Neuroimage* 47:1230–1236.
38. O'Rourke H, Fudge JL (2006) Distribution of serotonin transporter labeled fibers in amygdaloid subregions: Implications for mood disorders. *Biol Psychiatry* 60:479–490.
39. Gentleman RC, et al. (2004) Bioconductor: Open software development for computational biology and bioinformatics. *Genome Biol* 5:R80.
40. Gautier L, Cope L, Bolstad BM, Irizarry RA (2004) affy—analysis of Affymetrix GeneChip data at the probe level. *Bioinformatics* 20:307–315.
41. Lamballe F, Klein R, Barbacid M (1991) trkC, a new member of the trk family of tyrosine protein kinases, is a receptor for neurotrophin-3. *Cell* 66:967–979.
42. Duman CH, Duman RS (2005) Neurobiology and treatment of anxiety: Signal transduction and neural plasticity. *Handb Exp Pharmacol* 169:305–334.
43. Yamada M, et al. (1997) Insulin receptor substrate (IRS)-1 and IRS-2 are tyrosine-phosphorylated and associated with phosphatidylinositol 3-kinase in response to brain-derived neurotrophic factor in cultured cerebral cortical neurons. *J Biol Chem* 272:30334–30339.
44. van der Heide LP, Ramakers GMJ, Smidt MP (2006) Insulin signaling in the central nervous system: Learning to survive. *Prog Neurobiol* 79:205–221.
45. Lin CH, et al. (2001) A role for the PI-3 kinase signaling pathway in fear conditioning and synaptic plasticity in the amygdala. *Neuron* 31:841–851.
46. Ou L-C, Gean P-W (2006) Regulation of amygdala-dependent learning by brain-derived neurotrophic factor is mediated by extracellular signal-regulated kinase and phosphatidylinositol-3-kinase. *Neuropsychopharmacology* 31:287–296.
47. Mandai K, et al. (2009) LIG family receptor tyrosine kinase-associated proteins modulate growth factor signals during neural development. *Neuron* 63:614–627.
48. de Wit J, Hong W, Luo L, Ghosh A (2011) Role of leucine-rich repeat proteins in the development and function of neural circuits. *Annu Rev Cell Dev Biol* 27:697–729.
49. Feng Y, et al.; International Consortium for Childhood-Onset Mood Disorders (2008) Association of the neurotrophic tyrosine kinase receptor 3 (NTRK3) gene and childhood-onset mood disorders. *Am J Psychiatry* 165:610–616.
50. Armengol L, et al. (2002) 5′ UTR-region SNP in the NTRK3 gene is associated with panic disorder. *Mol Psychiatry* 7:928–930.
51. Alonso P, et al. (2008) Genetic susceptibility to obsessive-compulsive hoarding: The contribution of neurotrophic tyrosine kinase receptor type 3 gene. *Genes Brain Behav* 7:778–785.
52. Athanasiu L, et al. (2011) Intron 12 in NTRK3 is associated with bipolar disorder. *Psychiatry Res* 185:358–362.
53. Williams EJ (1959) The Comparison of Regression Variables. *J R Stat Soc Series B* 21: 396–399.
54. Zhang T-Y, Parent C, Weaver I, Meaney MJ (2004) Maternal programming of individual differences in defensive responses in the rat. *Ann N Y Acad Sci* 1032:85–103.
55. Turner CA, Clinton SM, Thompson RC, Watson SJ, Jr., Akil H (2011) Fibroblast growth factor-2 (FGF2) augmentation early in life alters hippocampal development and rescues the anxiety phenotype in vulnerable animals. *Proc Natl Acad Sci USA* 108: 8021–8025.
56. Upton KJ, Sullivan RM (2010) Defining age limits of the sensitive period for attachment learning in rat pups. *Dev Psychobiol* 52:453–464.
57. Sabatini MJ, et al. (2007) Amygdala gene expression correlates of social behavior in monkeys experiencing maternal separation. *J Neurosci* 27:3295–3304.
58. Russo SJ, et al. (2007) IRS2-Akt pathway in midbrain dopamine neurons regulates behavioral and cellular responses to opiates. *Nat Neurosci* 10:93–99.
59. Irvine EE, et al. (2011) Insulin receptor substrate 2 is a negative regulator of memory formation. *Learn Mem* 18:375–383.
60. Martín ED, et al. (2012) IRS-2 Deficiency impairs NMDA receptor-dependent long-term potentiation. *Cereb Cortex* 22:1717–1727.
61. White MF (2003) Insulin signaling in health and disease. *Science* 302:1710–1711.
62. Taguchi A, Wartschow LM, White MF (2007) Brain IRS2 signaling coordinates life span and nutrient homeostasis. *Science* 317:369–372.
63. den Heijer T, et al. (2003) Type 2 diabetes and atrophy of medial temporal lobe structures on brain MRI. *Diabetologia* 46:1604–1610.
64. Li C, et al. (2008) Diabetes and anxiety in US adults: Findings from the 2006 Behavioral Risk Factor Surveillance System. *Diabet Med* 25:878–881.
65. Peyrot M, Rubin RR (1997) Levels and risks of depression and anxiety symptomatology among diabetic adults. *Diabetes Care* 20:585–590.
66. Anderson RJ, Freedland KE, Clouse RE, Lustman PJ (2001) The prevalence of comorbid depression in adults with diabetes: A meta-analysis. *Diabetes Care* 24:1069–1078.
67. Caperuto LC, et al. (2006) Distinct regulation of IRS proteins in adipose tissue from obese aged and dexamethasone-treated rats. *Endocrine* 29:391–398.
68. Rojas FA, Hirata AE, Saad MJA (2003) Regulation of insulin receptor substrate-2 tyrosine phosphorylation in animal models of insulin resistance. *Endocrine* 21:115–122.
69. Paxinos G (2009) *The Rhesus Monkey Brain in Stereotaxic Coordinates* (Academic, Amsterdam, Boston, London), 2nd Ed. Copyright Academic Press (2009).

Supporting Information

Fox et al. 10.1073/pnas.1206723109

SI Methods

Subjects: Initial Assessment. Two hundred forty monkeys (*Macaca mulatta*) that were part of a large single-family pedigree were initially assessed using the NEC FDG-PET paradigm. Animals were mother-reared and pair-housed at the Harlow Primate Laboratory and the Wisconsin National Primate Research Center. At the time of initial assessment, the mean age was 2.4 y (range, 0.74–4.2 y). The typical lifespan of a rhesus macaque is ~25 y, and this age range would correspond to a human sample of mostly prepubescent children with some periadolescents. Animal housing and experimental procedures were in accordance with institutional guidelines. For additional details, see Oler et al. (1).

Subjects: Time 2 and Time 3 Assessments. Twenty-four male monkeys from the larger sample were assessed on two additional occasions using the NEC FDG-PET paradigm, for a total of three assessments over 6–18 mo. To ensure sufficient variance in Ce metabolic activity, animals were chosen to reflect the full spectrum of dorsal amygdala metabolism (Fig. 1*A*). The second and third assessments were separated by 21 d and varied in duration from initial assessment. Animals were 1.82–4.16 y old at second assessment (mean, 3.03; SD, 0.74). Between the second and third assessment half of the animals (6 high and 6 low) were relocated every 5 d. There were no significant effects of relocation on anxious behavior (*P* values, >0.05) or brain metabolism (*q* values, >0.05 FDR) in response to the NEC FDG-PET paradigm. All analyses treated brain metabolism and AT as continuous measures because quantile–quantile (QQ) plots revealed no strong deviations from normality.

FDG-PET Acquisition. Animals received i.v. injections of 5–10 mCi of FDG immediately before exposure to the 30-min NEC paradigm (described below), during which FDG-uptake occurred. After the NEC paradigm, subjects were anesthetized with 15 mg/kg ketamine intramuscularly for placement of an endotracheal tube, positioned in a stereotactic head-holder, and given isoflurane gas anesthesia (1–2%) for the duration of the 60-min scanning procedure, during which integrated FDG-uptake from the behavioral paradigm was measured. Scanning was performed using a microPET P4 scanner [Concorde Microsystems (2)] with an approximate resolution of 8 mm^3 [2-mm full width half max (FWHM)].

MRI Assessment. Magnetic resonance imaging (MRI) data were acquired after assessments 1 and 2 using a GE Signa 3T scanner (General Electric Medical Systems) with a standard quadrature birdcage headcoil using an axial 3D T1-weighted inversion-recovery fast gradient echo sequence [repetition time (TR): 9.4 ms; echo: 2.1 ms; field of view (FOV): 14 cm; flip: 10°; number of excitations: 2; in-plane: 0.2734 mm; 248 × 1 mm slices (−0.05-mm gap)]. Animals were anesthetized with an intramuscular injection of ketamine (15 mg/kg) before scanning. MRI data were collected within close temporal proximity to the NEC/FDG-PET session.

Serotonin Transporter Binding (DASB). The [^{11}C]DASB-PET methods are detailed elsewhere (3) and are only briefly described here. 3-[^{11}C]-Amino-4-(2-dimethylaminomethylphenylsulfanyl) benzonitrile (DASB) is a high-affinity ligand of serotonin transporter (5-HTT), and the carbon-11 for the radiolabeling was produced with a National Electrostatics 9SDH 6 MeV Van de Graff tandem accelerator. [^{11}C]DASB-PET data were acquired in 34 rhesus monkeys (mean age, 4.4 y; 12 male, 22 female) using a Concorde microPET P4 scanner (2). The dynamic PET time series were transformed into parametric images with each voxel representing the distribution volume ratio (DVR) serving as an index of receptor binding (4). The cerebellum was used as a reference region, and all voxel values were divided by the average cerebellar DASB binding value. Each subject's DVR image was transformed into standard space based on the corresponding MRI transformation. The group-averaged 5-HTT map was thresholded at 250× background cerebellar binding and used to demarcate the location of the lateral division of the Ce because compared with surrounding regions, the lateral division of the Ce has the highest density of 5-HTT binding (5).

Behavioral Paradigm: NEC Condition. During the NEC condition, FDG uptake occurred and behaviors were unobtrusively monitored. Animals were placed in a test cage and a human intruder entered the room and at a distance of 2.5 m, presenting her profile to the animal. Following 30 min of exposure to the intruder, animals were anesthetized and blood samples were collected. For more information, refer to Kalin and Shelton (6).

Behavioral and Cortisol Assessment. During the NEC condition, freezing was defined as a period of at least 3 s characterized by tense body posture, no vocalizations, and no locomotion except for slow movements of the head. Coo vocalizations were defined as audible calls made by rounding and pursing the lips with an increase and then decrease in frequency and intensity. Locomotion was defined as one or more full movements at any speed in any direction, including such behavior as dropping from ceiling to floor. Cortisol was measured in plasma samples using the Coat-A-Count cortisol RIA (Siemens Medical Solutions Diagnostics).

Creating the AT Composite. The composite measure of AT was calculated in two steps using SPSS (IBM SPSS Data Collection). First, each appropriately transformed measure [$-1 \times \text{cooing}^{1/2}$, cortisol, $\log_e$(freezing)] was residualized to remove variance linearly predicted by age. Note that cooing, which is associated with decreased anxiety in response to the NEC condition, was reversed to match cortisol and freezing, which are associated with increased anxiety. For cortisol, variance predicted by time-of-day was also removed. Second, composite AT was then computed as the mean of the three standardized (*Z*-transformed) residuals.

Tissue Isolation. After the animal was killed, the brain was removed and placed in a brain block. One hemisphere was cut into 4.5-mm-thick slabs for later biopsying of tissue, and the other hemisphere was cut into 14-mm slabs for subsequent sectioning on a cryostat. The brain slabbing was counterbalanced for hemisphere. Tissue slabs were stored at −80 °C before processing.

Functionally Guided Ce Biopsy. Slabs (4.5 mm) containing the Ce were identified, thawed briefly on wet ice, and placed on an inverted glass Petri dish on top of wet ice. A circular 3-mm punch tool was used to biopsy the region best corresponding to the Ce. Ce regions were identified from the coronal plane as the most dorsal portions of the amygdalar gray matter that were both (*i*) medial and ventral to the white-matter of the anterior commissure (AC) and (*ii*) lateral to the medial temporal convexity that houses the amygdalar cortical nuclei and the entorhinal cortex on the surface of the brain. The tissue punches were collected into 1.5-mL microfuge tubes and placed on dry ice. Samples were stored at –80 °C until analysis.

Microarray Gene Expression Assessment. RNA was extracted from each tissue punch using the RNeasy Plus Mini Kit (Qiagen). Labeled cRNA was then prepared using the 3′ IVT Express Kit (Affymetrix) and hybridized to Affymetrix GeneChip Rhesus Macaque Genome arrays.

qRT-PCR Gene Expression Assessment. The same RNA used for the gene chip analysis served as template to prepare cDNA using SuperScript Vilo (Life Technologies). Selected genes were confirmed using qRT-PCR with TaqMan probes (Applied Biosystems). Resulting expression values were log-scaled and normalized to levels of *succinate dehydrogenase complex, subunit A, flavoprotein* (*Fp*) (*SDHA*). Two subjects were excluded from these analyses, because of issues regarding RNA yield and quantification.

AChE Assessment. AChE staining was based on a published method (7). Briefly, slides were incubated for 2 h in 0.12% acetyl thiocholine iodide, 0.0072% ethopropazine, 0.075% glycine, 0.05% cupric sulfate, and 0.68% sodium acetate. Following three rinses in water, the slides were immersed in 0.77% sodium sulfide for 30 min and washed three times in water. The stain was then developed for 10 min in 1% silver nitrate protected from light. Following dehydration in ethanol and clearing in xylene, the slides were mounted using DPX mountant.

In Situ NTRK3 Assessment. Ce *NTRK3* expression was confirmed by in situ hybridization. To accurately localize Ce, AChE staining was performed on a coronal slice immediately posterior to that used for the *NTRK3* mRNA stain. Ce regions were defined on the AChE stain using the Paxinos atlas (8). The 499-bp rhesus *NTRK3* probe was amplified from rhesus amygdala cDNA using forward (5′-GAATAGAGTCTATGCCTTTGGCAAA-3′) and reverse (5′-TCTCTGTGGAAACACAACG-3′) PCR primers. The sequence was based on the Affymetrix probe set MmugDNA.29582.1.S1_at and was 98% identical to the human *NTRK3* sequence (GenBank accession no. NM_001007156). The PCR product was subcloned into pBluescript II SK(+) (Agilent Technologies) that had been digested with KpnI and SacI (New England Biolabs). The *NTRK3*-pBluescript plasmid was linearized with Acc65I (New England Biolabs) and transcribed and labeled with [α-^{35}S]UTP (Perkin-Elmer) using T3 RNA polymerase with the Riboprobe Combination System (Promega). The labeled probe was purified using ProbeQuant G-50 Micro Columns (GE Healthcare). The slide-mounted brain sections were fixed in 4% paraformaldehyde before being permeabilized with proteinase K. Following acetylation with acetic anhydride and triethanolamine, the tissue was hybridized with the labeled probe overnight at 55 °C. The tissue was treated with RNase A before being washed and exposed to a phosphor screen. Screens were scanned using Typhoon 9410 (GE Healthcare), and the signal was quantified using ImageQuant 5.2 software (GE Healthcare).

FDG-PET Preprocessing. Methods were similar to our prior work (1). Each subject's T1-MRI was manually stripped of extracerebral tissue using SPAMALIZE (http://brainimaging.waisman.wisc.edu/~oakes/spam). Skull-stripped images were registered to a 34-brain template in standard space (8, 9) (12-parameter linear) using FLIRT (http://www.fmrib.ox.ac.uk/fsl/flirt) and manually verified. Images from the large sample were averaged to create a study-specific, 238-brain template in standard space (8). Skull-stripped images were registered to this template using FNIRT (http://fsl.fmrib.ox.ac.uk/fsl/fnirt). Resulting standard-space images were corrected for spatial radiofrequency (RF) inhomogeneities and segmented into gray matter, white matter, and cerebrospinal fluid probabilities using FAST (http://www.fmrib.ox.ac.uk/fsl/fast4). To spatially normalize FDG-PET images, we concatenated two transformation matrices: the matrix generated by registering each animal's FDG-PET to its own T1-MRI (six-parameter linear) and the MRI-to-template matrix described above. The concatenated matrix was applied to the FDG-PET images. FDG-PET image intensities were scaled to the global mean signal across the region defined by their skull-stripped T1-MRI. Scaled FDG-PET images and GMP maps were spatially smoothed (4-mm FWHM). Mean FDG-PET images were created in standard space by taking the voxel-wise mean across FDG-PET assessments.

Microarray Gene Expression Preprocessing. Gene expression data were analyzed using R (http://cran.r-project.org) and the bioconductor libraries for microarray analysis [http://www.bioconductor.org/; version 2.7 (10)]. Microarray expression values were corrected for background noise using the RMA algorithm, levels of gene expression were normalized across chips with a constant, mismatch probes were ignored, and expression data were summarized across probes using the median-polish technique (11). Gene expression levels were visually inspected using MA plots (Fig. S1). To ensure results were not an artifact of normalization, gene xpression was also quantified using Plier background correction and quantile normalization across arrays. Both normalization techniques revealed similar distributions of gene expression across chips. Because AT is likely to be highly polygenic (12), the quantile normalization, which matches overall gene distribution, may be inappropriate. Therefore, the constant normalization method was used in all analyses. Resulting expression estimates for each probe set were filtered using mean expression levels; subthreshold probe sets [$<\log_2(100)$] were excluded. Genes were annotated using publicly available annotations verified by BLASTing against the human genome by the University of Nebraska Non Human Primate Genomics Center, which developed the Rhesus Monkey microarray chip in collaboration with Affymetrix (http://www.unmc.edu/rhesusgenechip/).

FDG-PET Statistical Analyses. Voxel-wise analyses were performed using an adaptation (13) of Fmristat (http://www.math.mcgill.ca/keith/fmristat/) (14, 15). Regressions were performed across the whole brain and, when applicable, controlling for age, change in age across assessments, sex, relocation, and voxel-wise GMP. Initial voxel-wise screening for AT-related voxels was reported in Oler et al. (1). Control analyses revealed that results did not substantively change when GMP was omitted from our regressions, confirming the lack of influence of any gray matter differences on the observed relations with metabolic activity.

Identifying regions with stable brain metabolism. To identify stable metabolism in regions predictive of AT, we performed voxel-wise regressions between each pair of longitudinal FDG-PET scans, controlling for age, change in age, relocation, and GMP. Regions surviving FDR correction ($q \leq 0.05$, two-tailed across three maps) within previously identified AT-related regions in each of the three pairwise comparisons [equivalent to logical AND conjunction (16)] were identified as stable. We also computed voxel-wise $ICC_{3,1}$ values to assess test–retest reliability (17). $ICC_{3,1}$ values were computed across the three FDG-PET assessments, controlling for age, change in age, relocation, and GMP. Results are shown in Table S1. It is important to note that significant stability should be interpreted as relative stability rather than invariance.

Identifying stable AT-related regions. Stable components of AT and brain metabolism were computed by averaging across the three assessments. Mean AT was then correlated with mean metabolism within metabolically stable regions (see above), controlling for mean age, relocation, and mean GMP. Maps were thresholded using FDR ($q \leq 0.05$, two-tailed) within stable regions. Results are shown in Table S2.

Identifying locomotion-related regions. Locomotion-related brain regions were identified using the same procedures used for AT but using individual differences in locomotion during the NEC condition as an explanatory variable. A voxel-wise regression was

computed between mean locomotion and the corresponding brain metabolism in the 238 animals described in Oler et al. (1), controlling for age, sex, and GMP. Results were thresholded using the Sidak procedure. This revealed reliable associations between locomotion and metabolic activity in motor cortex (Table S7)

Microarray Gene Expression Statistical Analyses. The primary analysis of interest was the relationship between mean AT across the three assessments and individual differences in gene expression levels. Microarray analyses were performed using robust regression. Robust regression attenuates the influence of high-leverage outliers, minimizing the likelihood that a small number of observations exerted disproportionate effects on the β estimate. Regression analyses were performed between mean AT and all probe sets that were abundant [$>\log_2(100)$] and annotated. Statistical significance was assessed using an empirical Bayes method (18) and corrected for multiple comparisons using FDR ($q \leq 0.05$, two-tailed). Results revealed 148 probe-sets representing 139 genes, which are shown in Table S3. To ensure that results were not simply reflecting the normalization procedure, the same statistical analyses were performed on quantile and Plier normalized data. Results from Plier background-corrected and quantile-normalized gene-AT analyses are reported in Table S3 for each gene that was significant using RMA background correction and constant normalization. Probe sets that were confirmed with PCR were further validated by BLAST probe sets against the rhesus monkey genome.

To identify sets of genes that were overrepresented in our list of 139 significant genes, we performed gene set enrichment analyses on gene ontologies using weighted correlation network analysis (WGCNA) and GOTools packages in R. We examined the number of significant (FDR $q < 0.05$) genes in each term within the HomoSapien ontology database (Table S4). This was performed on each term within each of the three gene ontologies in the gene ontology database (Molecular Function, Cellular Component, and Biological Processes) by computing Fisher's exact test on a table with genes falling into the four bins of a Significant (Yes/No) by In-Term (Yes/No) cross-tabulation. This test is equivalent to a one-tailed hypergeometric test. Additionally, to ensure that our inferences were not influenced by the false negatives resulting from our stringent multiple comparison correction, we performed the same ontology enrichment analyses for the set of genes that predicted AT at a significant ($P < 0.05$) uncorrected threshold (Table S5).

qRT-PCR Gene Expression Statistical Analyses. qRT-PCR–measured gene expression levels were regressed against AT using the same methods applied to the microarray data (see above).

Assessing the relationship between gene expression and stable AT-related metabolism. Voxel-wise regressions were performed between qRT-PCR–measured Ce *NTRK3* gene expression levels and mean FDG-PET across three assessments, controlling for mean age, relocation, and mean GMP. Resulting maps were thresholded using FDR ($q \leq 0.05$, two-tailed) in stable AT-related regions. Results are shown in Table S6. Similar analyses were performed for qRT-PCR–measured motor cortex *NTRK3* gene expression levels and mean FDG-PET in AT-related regions. Results demonstrated no significant effects.

Assessing the relationship between gene expression and locomotion-related metabolism. Voxel-wise regression were performed between qRT-PCR–measured motor cortex *NTRK3* gene expression levels and mean FDG-PET across the three assessments controlling for mean age, relocation, and mean GMP. Resulting maps were corrected for multiple comparisons using FDR ($q \leq 0.05$, two-tailed) in stable locomotion-related regions described above. This analysis revealed no significant results.

1. Oler JA, et al. (2010) Amygdalar and hippocampal substrates of anxious temperament differ in their heritability. *Nature* 466:864–868.
2. Tai C, et al. (2001) Performance evaluation of the microPET P4: A PET system dedicated to animal imaging. *Phys Med Biol* 46:1845–1862.
3. Christian BT, et al. (2009) Serotonin transporter binding and genotype in the nonhuman primate brain using [C-11]DASB PET. *Neuroimage* 47:1230–1236.
4. Innis RB, et al. (2007) Consensus nomenclature for in vivo imaging of reversibly binding radioligands. *J Cereb Blood Flow Metab* 27:1533–1539.
5. O'Rourke H, Fudge JL (2006) Distribution of serotonin transporter labeled fibers in amygdaloid subregions: Implications for mood disorders. *Biol Psychiatry* 60: 479–490.
6. Kalin NH, Shelton SE (1989) Defensive behaviors in infant rhesus monkeys: Environmental cues and neurochemical regulation. *Science* 243:1718–1721.
7. Lim MM, Hammock EAD, Young LJ (2004) A method for acetylcholinesterase staining of brain sections previously processed for receptor autoradiography. *Biotech Histochem* 79:11–16.
8. Paxinos G (2009) *The Rhesus Monkey Brain in Stereotaxic Coordinates* (Academic, Amsterdam, Boston, London), 2nd Ed.
9. Fox AS, Shelton SE, Oakes TR, Davidson RJ, Kalin NH (2008) Trait-like brain activity during adolescence predicts anxious temperament in primates. *PLoS ONE* 3:e2570.
10. Gentleman RC, et al. (2004) Bioconductor: Open software development for computational biology and bioinformatics. *Genome Biol* 5:R80.
11. Gautier L, Cope L, Bolstad BM, Irizarry RA (2004) affy—analysis of Affymetrix GeneChip data at the probe level. *Bioinformatics* 20:307–315.
12. Flint J (2001) Psychiatric genetics: A frightful chromosome. *Curr Biol* 11:R907–R909.
13. Oakes TR, et al. (2007) Integrating VBM into the General Linear Model with voxelwise anatomical covariates. *Neuroimage* 34:500–508.
14. Friston KJ, et al. (1995) Analysis of fMRI time-series revisited. *Neuroimage* 2:45–53.
15. Worsley KJ, Poline JB, Friston KJ, Evans AC (1997) Characterizing the response of PET and fMRI data using multivariate linear models. *Neuroimage* 6:305–319.
16. Nichols T, Brett M, Andersson J, Wager T, Poline J-B (2005) Valid conjunction inference with the minimum statistic. *Neuroimage* 25:653–660.
17. Shrout PE, Fleiss JL (1979) Intraclass correlations: Uses in assessing rater reliability. *Psychol Bull* 86:420–428.
18. Smyth GK (2004) Linear models and empirical bayes methods for assessing differential expression in microarray experiments. *Stat Appl Genet Mol Biol* 3:Article3.

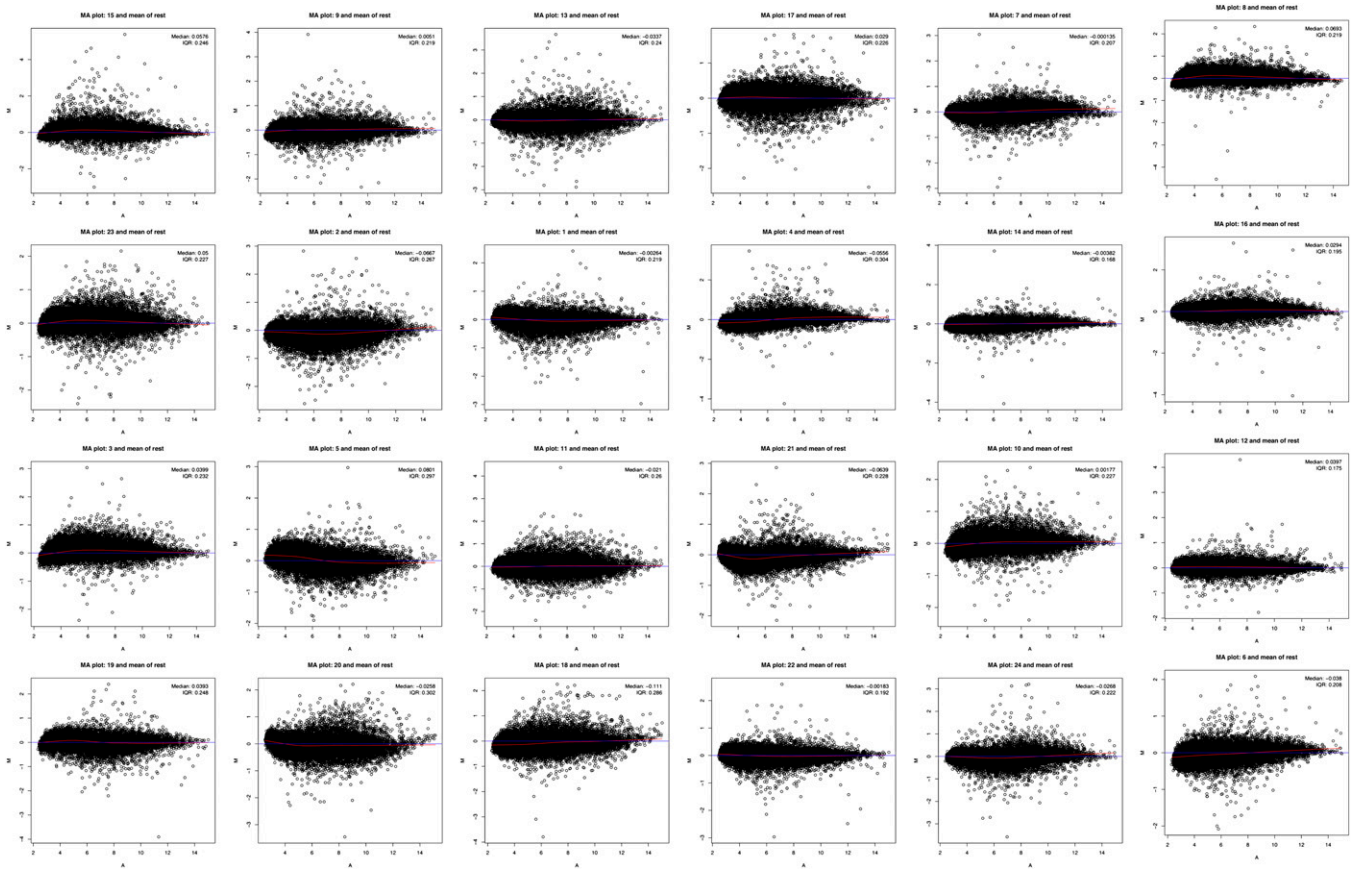

Fig. S1. Limited nonlinear distortion demonstrated using MA plots showing the relationship between the average of each chip and the mean of the other chips (A) and the difference between that chip and the mean of the other chips (M). The chips are ordered by AT from left to right and top to bottom, with the lowest AT subject in the upper-left corner and the highest AT subject in the lower-right corner.

Other Supporting Information Files

Table S1 (XLSX)
Table S2 (XLSX)
Table S3 (XLSX)
Table S4 (XLSX)
Table S5 (XLSX)
Table S6 (XLSX)
Table S7 (XLSX)